AIAA JOURNAL
Vol. 33, No. 7, July 1995

# Control of Shock-Wave/Boundary-Layer Interactions by Bleed

W. J. Chyu*
*NASA Ames Research Center, Moffett Field, California 94035*
and
M. J. Rimlinger† and T. I-P. Shih‡
*Carnegie Mellon University, Pittsburgh, Pennsylvania 15213-3890*

**This numerical study investigates the effectiveness of bleed in controlling shock-wave/boundary-layer interactions on a flat plate with a focus on understanding how bleed-hole angle, presence of upstream and downstream bleed holes, and pressure ratio across bleed holes affect structure of "barrier" shock, surface pressure distribution, and bleed rate (in terms of flow coefficient). The bleed-hole angles investigated are 30 deg slanted and 90 deg normal, which give rise to two different types of barrier shocks. The influence of upstream and downstream bleed holes were investigated by studying the bleed process through an isolated hole and through three holes arranged in tandem along the streamwise direction. The plenum/freestream pressure ratios investigated range from 0.3 to 1.7, which produced choked and unchoked flows in the bleed holes. This study is based on the ensemble-averaged, full compressible Navier–Stokes equations closed by the Baldwin–Lomax model with solutions obtained by an implicit finite volume method on an overlapping Chimera grid.**

## Introduction

EFFECTIVE control of shock-wave/boundary-layer interactions is important in many applications. Examples include mixed-compression supersonic inlets, transonic wind tunnels, and airframes of supersonic aircraft. This is because when a shock wave strikes a boundary layer, a number of adverse effects can result, including flow separation.[1] One effective way of controlling these adverse effects is to place bleed holes in the vicinity where the shock wave strikes the boundary layer.[2] Though this method of control is effective, it reduces efficiency by removing air from the main stream. Thus, the goal in designing bleed-hole systems is to bring about the most effective control with the least amount of bleed.

The importance of bleed in controlling shock-wave/boundary-layer interactions has led a number of investigators to use experimental and numerical methods to study this problem. To date, only numerical studies have reported the detailed flowfield in and around the bleed holes.[3–9] Such information is critical to understanding the details of the bleed process as a function of bleed-hole design parameters. Of these studies, only Shih et al.[9] investigated three-dimensional, shock-wave/boundary-layer interactions with bleed. They investigated oblique-shock-wave/boundary-layer interactions on a flat plate fitted with a single circular hole that bled the flow above the plate into a plenum. Their study showed that if the plenum pressure is sufficiently low, then a two-segment "barrier" shock forms in and on the downstream edge of the bleed hole. The authors noted that this barrier shock can block information downstream of it from propagating upstream and, hence, is another mechanism that can be utilized to prevent flow separation (i.e., the barrier shock can be utilized in addition to the mechanism of removing low-momentum air next to solid surfaces). The authors further noted that the barrier shock also increases mixing above the plate because it disrupts the flow locally by slowing it down and increasing its static pressure. This increased mixing is still another mechanism that can be utilized to prevent flow-separation and to bring about a more uniform flow downstream of the shock-wave/boundary-layer interaction region.

At this point, it should be noted that the study by Shih et al.[9] on the formation of the barrier shock and its properties only investigated one bleed-hole geometry and one plenum back pressure. In the present paper, the focus is on understanding how bleed-hole angle, presence of an upstream and a downstream bleed hole, and pressure ratio across bleed holes affect the structure of the barrier shock, surface pressure distribution, and bleed rate (given in terms of the flow coefficient). Although only two bleed-hole angles (90 and 30 deg) and two different numbers of bleed holes (either 1 or 3) were investigated, their selection was made to illustrate the full range in the nature of the flow. The two bleed-hole angles were selected to show the maximum variations that can take place in the barrier shock structure due to bleed-hole angle. The reason that the number of bleed holes is either one or three is to show the difference between an isolated single bleed hole and holes that are surrounded by neighboring holes in the streamwise direction. Finally, since small changes in plenum pressure can have substantial effects on the barrier shock structure and the bleed process, five different plenum/freestream pressure ratios were investigated ranging from 0.3 to 1.7 in order to examine both choked and unchoked flows in the bleed holes. For each pressure ratio, both 90- and 30-deg holes and both single and holes-in-tandem were investigated.

## Description of Problem

A schematic diagram of the bleed-hole problem studied is shown in Fig. 1. The domain of this problem is the region bounded by the dashed lines which includes the region above the flat plate, the bleed holes, and the plenum. All dimensions in Fig. 1 are given in terms of $D$, which is the diameter of the bleed hole and is 0.003175 m ($\frac{1}{8}$ in.).

Several variations of the configuration shown in Fig. 1 were investigated. The first variation is that the angle of the bleed hole ($\alpha$ in Fig. 1) can be 90 deg normal or 30 deg slanted. Note that when a bleed hole is normal, the cross section of that bleed hole in a plane parallel to the plate is a circle. But, when a bleed hole is slanted, the cross section of that bleed hole is an ellipse, as shown in Fig. 1. The second variation is that the number of bleed holes can be either three as shown in Fig. 1 or just one. When there are three bleed holes, the spacing between the centers of the bleed holes (S in Fig. 1) was $2D$ for 90-deg holes and $4D$ for 30-deg holes. The location of the middle hole is always located at $32.5D$ from the inflow boundary. When there is only one hole, the location of that hole coincided with the middle hole of the three-hole cases.

Presented as Paper 93-3259 at the AIAA Shear Flow Conference, Orlando, FL, July 6–9, 1993; received July 30, 1994; revision received Dec. 9, 1994; accepted for publication Dec. 12, 1994. Copyright © 1995 by the American Institute of Aeronautics and Astronautics, Inc. No copyright is asserted in the United States under Title 17, U.S. Code. The U.S. Government has a royalty-free license to exercise all rights under the copyright claimed herein for Governmental purposes. All other rights are reserved by the copyright owner.

*Research Scientist, Applied Aerodynamics Branch. Member AIAA.
†Graduate Student, Department of Mechanical Engineering.
‡Professor, Department of Mechanical Engineering. Member AIAA.

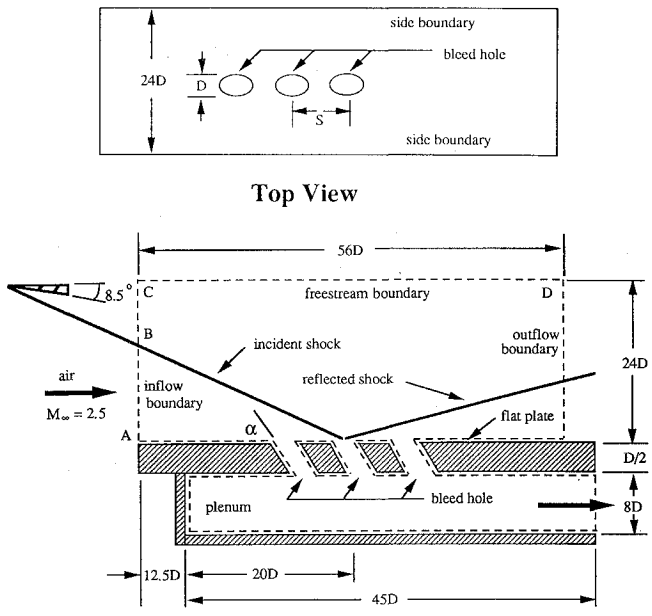


**Fig. 1 Schematic diagram of bleed-hole problem studied.**

For the bleed-hole problem and its variations just described, the fluid that enters the domain above the flat plate is air with a constant specific-heats ratio $\gamma$ of 1.4. The freestream Mach number $M_\infty$, static temperature $T_\infty$, and density $\rho_\infty$ are 2.5, 134 K, and 0.262 kg/m$^3$, respectively. This supersonic flow has a turbulent, boundary layer next to the flat plate. At the inflow boundary, the thickness of that boundary layer $\delta$ is 0.003175 m ($\frac{1}{8}$ in.), which is equal to the diameter of the bleed holes.

A shock-wave generator causes an oblique-shock wave to strike the turbulent boundary layer on the flat plate. The shock wave generated is strong enough to induce flow separation on the flat plate when there is no bleed. The shock-wave generator is positioned so that the oblique shock strikes the flat plate at $32.5D$ from the inflow boundary under inviscid conditions. This corresponds to the center of the middle hole for three-hole cases, and the center of the isolated hole for one-hole cases.

To study the effects of pressure ratio across bleed holes, the following back pressures $P_b$ at the exit of the plenum were investigated: $0.3P_\infty$, $0.6P_\infty$, $0.9P_\infty$, $1.3P_\infty$, and $1.7P_\infty$, where $P_\infty$ is the freestream static pressure which can be calculated from the freestream temperature and density. When there was no bleed, the static pressure at the center of the bleed hole or at the center of the middle bleed hole was $1.75P_\infty$.

## Formulation of Problem

The flow problem described in the previous section was modeled by the density-weighted, ensemble-averaged conservation equations of mass, momentum (full compressible Navier–Stokes), and total energy written in generalized coordinates and cast in strong conservation-law form. The effects of turbulence were modeled by the Baldwin–Lomax[10] algebraic turbulence model. Justification for using such a simple turbulence model is as follows. First, algebraic models are known to give good results when there are no flow separation, which is the case here on the flat plate in the vicinity of the holes because of the bleed. Second, the point of separation in the bleed hole, which is critical in determining the structure of the barrier shock, is primarily controlled by sudden changes in geometry (basically, along flat plate and then, suddenly, into hole), instead of turbulence.

To obtain solutions to the conservation equations, boundary and initial conditions are needed. The boundary conditions (BCs) employed in this study for the different boundaries shown in Fig. 1 are as follows. At the inflow boundary where the flow is supersonic everywhere except for a very small region next to the flat plate, two types of BCs were imposed. Along segment A–B, all flow variables were specified at the freestream conditions except for the streamwise velocity which had a turbulent boundary layer described by the van Driest profile in the inner layer and the one-seventh power law in the outer layer. With such a velocity profile, the displacement and momentum thicknesses corresponding to a boundary-layer thickness of 0.003175 m ($\frac{1}{8}$-in.) are 0.003 m and 0.0015 m, respectively. The Reynolds number based on the displacement thickness at the inflow boundary was 60,000. Along segment B–C, postshock conditions based on inviscid, oblique, shock-wave theory were specified. These postshock conditions were also specified along the freestream boundary (segment C–D). At the outflow boundary where the reflected shock wave exited the computational domain, the flow is also mostly supersonic except for a small region next to the wall so that all flow variables were extrapolated by using linear extrapolation based on three-point, backward differencing. The BCs imposed at the two side boundaries above the flat plate were the same as the ones imposed at the outflow boundary. At the exit of the plenum where the flow is subsonic, a back pressure $P_b$ was imposed, and density and velocity were extrapolated in the same manner as the variables at the outflow boundary. As noted in the section on problem description, several different values of $P_b$ were investigated.

At all solid walls except for the two side walls of the plenum, the no-slip condition, adiabatic walls, and zero normal-pressure gradient were imposed. At the two side walls of the plenum, the following inviscid wall BC was applied: the normal component of the velocity was set to zero; the first-derivative of the tangential component of the velocity normal to the wall was taken to be zero; the wall was adiabatic; and the normal momentum equation was used to determine pressure. This inviscid wall BC was imposed because boundary-layer flows next to those two boundaries do not affect appreciably the bleed process, and treating them as inviscid walls reduces computational cost by requiring fewer grid points next to those boundaries.

Even though only steady-state solutions were of interest, initial conditions were needed because the unsteady form of the conservation equations was used. The initial conditions employed in this study are as follows. In the region above the flat plate, the initial condition was the two-dimensional, steady-state solution for an incident and a reflected oblique shock wave on a flat plate based on inviscid, oblique, shock-wave theory. The streamwise velocity profile, however, was modified to give the van Driest/one-seventh power-law profile. This necessitated the total energy per unit volume to be modified as well in order to account for the change in mechanical energy within the boundary layer. The initial conditions used in each bleed hole and in the plenum were stagnant air with density $\rho_\infty$ at constant pressure $P_b$.

At this point, it is important to note that the problem described in the previous section appears to be symmetric about a plane that is perpendicular to the flat plate and passes through the centers of the bleed holes. This symmetry was not invoked in order to study the possibility of asymmetry that may result from the wake behind the jet-like flow into the bleed holes.

## Numerical Method of Solution

Solutions to the ensemble-averaged conservation equations of mass, momentum, and total energy closed by the Baldwin–Lomax algebraic turbulence model described in the previous section were obtained by using the OVERFLOW code.[11] The OVERFLOW code contains many algorithms. The one used in this study is as follows. Inviscid-flux terms in the $\xi$ direction (which was aligned with the flow direction as much as possible) were upwind differenced by using the flux-vector splitting procedure of Steger and Warming.[12] Inviscid-flux terms in directions normal to the $\xi$ direction were centrally differenced in order to reduce artificial dissipation in those direction. All diffusion terms were also centrally differenced. The time-derivative terms were approximated by the Euler implicit formula. This low-order accurate formula was used because only steady-state or quasi-steady-state solutions are sought here. The system of nonlinear equations that resulted from the aforementioned approximations to the space- and time-derivatives were analyzed by using the partially split method of Steger et al.[13] In

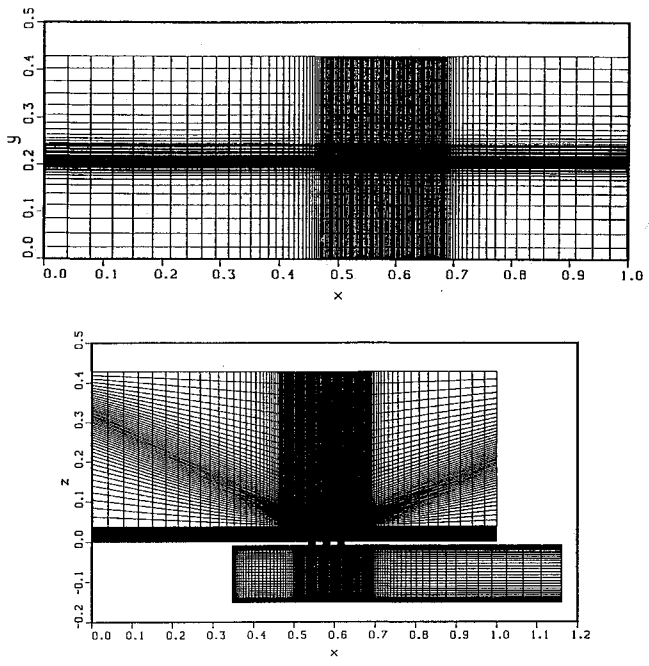


**Fig. 2 Grid system used for the case with three 90-deg holes.**

OVERFLOW, Jacobians and metric coefficients are interpreted as grid-cell volumes and grid-cell surface areas, respectively. In this regard, all algorithms in OVERFLOW are implemented in the finite volume manner. However, BCs in OVERFLOW are implemented in a finite difference manner in order to enhance flexibility and ease in investigating different problems.

For the bleed-hole problem shown in Fig. 1 and its variations which are not shown, the computational domain was always divided into a number of zones, each with a different coordinate system in order to align upwind differencing with the streamwise direction. For this multizone computational domain, a Chimera grid system with several overlapping grids was employed. An example of the grid system employed is shown in Fig. 2 for the configuration with three 90-deg holes (similar grids were generated for the case with three 30-deg holes and for cases with only one 90- or one 30-deg hole). Note that in that figure, the spatial dimensions were nondimensionalized by $56D$ (which is equal to 0.1778 m) as indicated by the coordinate system. The purpose of this coordinate system is to show the location in the computational domain where data is provided.

For the zone above the flat plate, the grid system used was a single-solution adapted H–H grid (adaptation was based on the initial conditions) which had grid points clustered near the flat plate, bleed hole, and the impinging and reflected shock waves (Fig. 2). The number of grid lines used in this H–H grid were as follows: 155 grid lines from inflow to outflow, 101 grid lines from plate to freestream boundary, and 51 grid lines from side boundary to side boundary. The grid spacings in the streamwise direction varied from $7.112 \times 10^{-3}$ m at the inflow boundary to $4.196 \times 10^{-4}$ m at a distance of 0.0238 m before where the shock wave would impinge on the plate under inviscid conditions. From 0.0238 m before the inviscid shock impingement point to 0.0238 m after that point, the grid spacings in the streamwise direction were kept constant at $3.664 \times 10^{-4}$ m. From 0.0238 m after the shock impingement point to the outflow boundary, the grid spacings varied from $4.196 \times 10^{-3}$ m to $5.334 \times 10^{-4}$ m. The grid spacings in the direction normal to plate varied from $3.556 \times 10^{-5}$ m at the plate to $3.556 \times 10^{-3}$ m at the freestream boundary. The grid spacing in the spanwise direction was kept constant at $3.664 \times 10^{-4}$ m in the region between 0.00513 m before and after the center of the bleed hole. Once outside of that region, the grid spacings were increased steadily until they reached a value of $4.445 \times 10^{-3}$ m at the two side boundaries.

For the zones containing the bleed hole, two overlapping grids were used, an O–H grid touching the wall the bleed hole and an H–H grid at the center of the bleed hole.[9] The O–H grid with $20 \times 37 \times 21$ grid points was used to resolve the circular geometry of the bleed hole. The H–H grid with $20 \times 21 \times 21$ grid points was used to eliminate the centerline singularity associated with the O–H grid. For the zone containing the plenum, a single H–H grid was used (Fig. 2). This H–H grid had $81 \times 51 \times 50$ grid points with grid points clustered near walls and the bleed hole or holes. Note that grid spacings in different grids were made comparable in regions where they overlapped in order to minimize aliasing errors.

The grid system just described was generated by using algebraic grid generation with Vinokur's one-dimensional stretching functions.[14] The clustering and the number of grid points employed were arrived at after considerable numerical experiments to ensure grid-independent solutions for the bleed rates and the pressures on the top surface of the flat plate.

During computations, the flowfield in each grid was analyzed one at a time in the following order: 1) the H–H grid above the flat plate, 2) the H–H grid in the bleed hole, 3) the O–H grid in the bleed hole, 4) repeat 2 and 3 for all bleed holes, and 5) the H–H grid in the plenum. Information from one grid was passed to another grid via trilinear interpolation at grid boundaries in the overlapped regions. The required interpolation coefficients were obtained by using the PEGSUS code.[15] This process of analyzing the flow in one grid at a time until all grids are analyzed was repeated for each time step until a converged solution was obtained. Here, a solution is assumed to be converged if the second norm of the residual leveled out for at least 500 time steps. Typically, at that time, the second norm is about $10^{-7}$. Here, it is noted that the residual oscillated about some averaged value as it leveled out, but the amplitude of those oscillations were less than $10^{-7}$.

## Results

Numerical solutions were obtained to investigate the effectiveness of bleed in controlling shock-wave/boundary-layer interactions on a flat plate. The focus is on understanding how bleed-hole angle, presence of an upstream and a downstream bleed hole, and pressure ratio across bleed holes affect structure of barrier shock, surface pressure distribution, and flow coefficient. The bleed-hole angles investigated are 30 deg slanted and 90 deg normal. Proximity of bleed holes to each other was studied by having bleed through only one 90- or 30-deg hole and by having bleed through three 90- or three 30-deg holes that are arranged in tandem. Whether there is one hole or three holes and whether the hole is 90- or 30-deg, five different pressure ratios $P_b/P_\infty$ were investigated, and they are 0.3, 0.6, 0.9, 1.3, and 1.7 (recall that the static pressure at the center of the isolated hole or the center of the middle hole was $1.75P_\infty$ in the absence of bleed). For each of these pressure ratios, only $P_b$ was changed with $P_\infty$ kept constant. This is to ensure that the flow above the flat plate in the absence of bleed can be used as a reference about which comparisons can be made.

Results of this study are given in Figs. 3–11. Before describing these results in detail, note that they are given along two planes, one seen from the side and the other from the top. For the side view, the $x$–$z$ plane is perpendicular to the flat plate and passes through the center or centers of the bleed hole or holes as well as the centers of the inflow and outflow boundaries. For the top view, the $x$–$y$ plane is parallel to the flat plate and 0.0001953 m (0.00769 in.) above it. For each figure, a coordinate system is attached which shows its relative size and location in the domain. Also, note that the flow coefficient as used here is defined as the actual bleed rate divided by an ideal bleed rate. The ideal bleed rate assumes sonic flow in the entire bleed hole with stagnation pressure and temperature equal to those outside of the boundary layer.

### Effects of Bleed-Hole Angle

Figures 3 and 4 show Mach number contours with bleed through a single 90- and 30-deg hole, respectively, at a pressure ratio $P_b/P_\infty$ of 0.3 in the region about the bleed hole. Figure 3 shows that for the 90-deg hole, the two-segment barrier shock is detached (i.e., it is a bow shock) and extends from inside the bleed hole to above the plate and downstream of the bleed hole. A schematic of this shock structure is shown in Fig. 5a. Figure 4 shows that for the 30-deg hole, the barrier shock has only one of the two segments, the one

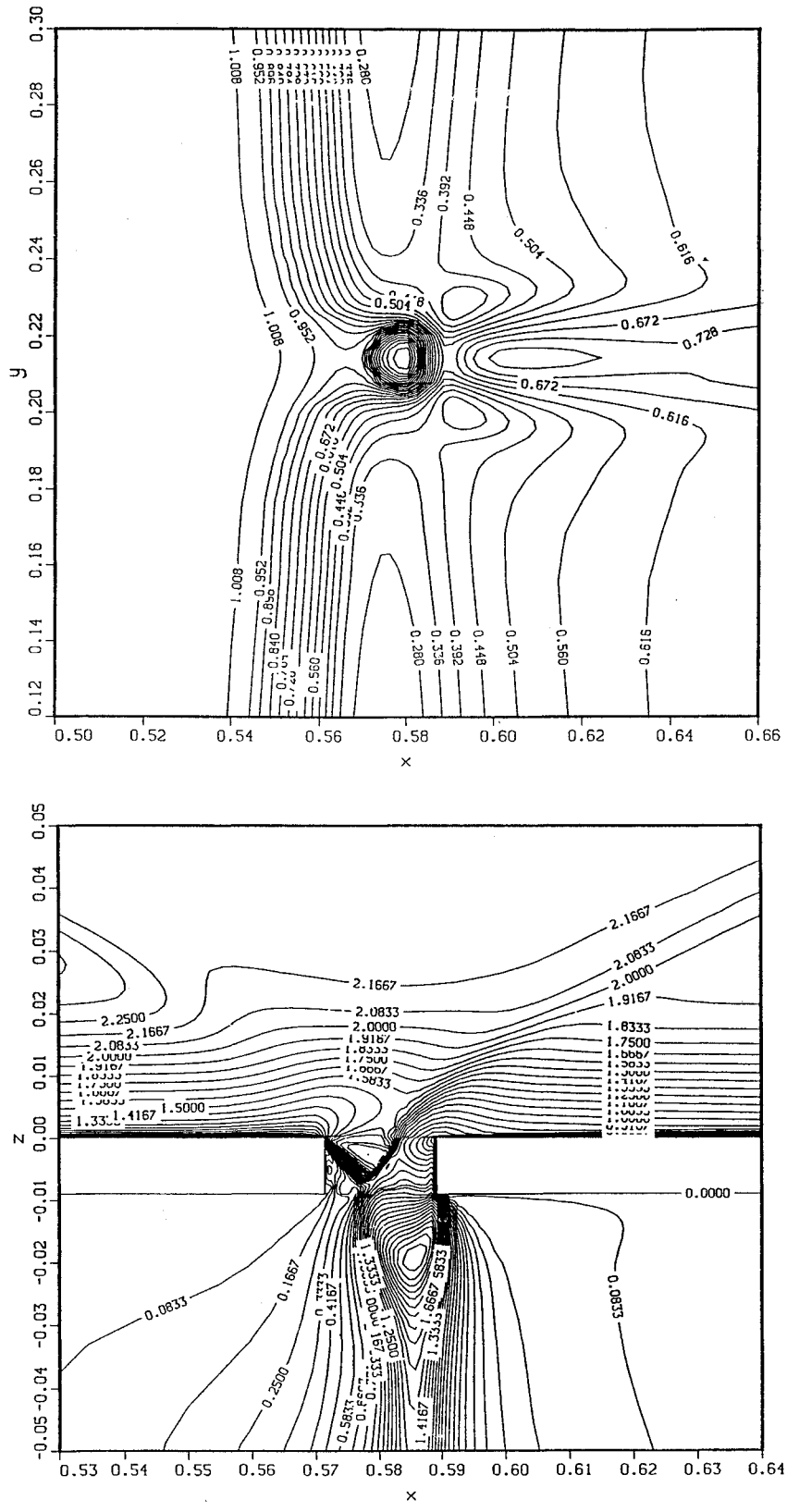


**Fig. 3 Mach number contours near the bleed hole for the case with a single 90-deg bleed hole and $P_b/P_\infty = 0.3$, top and side views.**

above the flat plate which extends from the surface of the flat plate to above the plate and downstream of the bleed hole. For this bleed-hole angle, the turning of the supersonic flow into the bleed hole is insufficient for the compression waves to coalesce into an oblique shock wave in the bleed hole. A schematic of this shock structure is shown in Fig. 5b. Thus, it can be seen that the angle of the bleed hole affects significantly the structure of the barrier shock and the flow around it.

Figures 3 and 4 also show the influence exerted by a bleed hole in the spanwise and downstream directions as a function of bleed-hole angle. From these figures, it can be seen that bleed can change the position of the bow shock formed ahead of the separation bubble with the 30-deg hole producing a greater change than the 90-deg hole. This change in position occurs because bleed changes the size of the separation bubble in the spanwise direction. That size changes from zero (i.e., no separated region) at the bleed hole to a

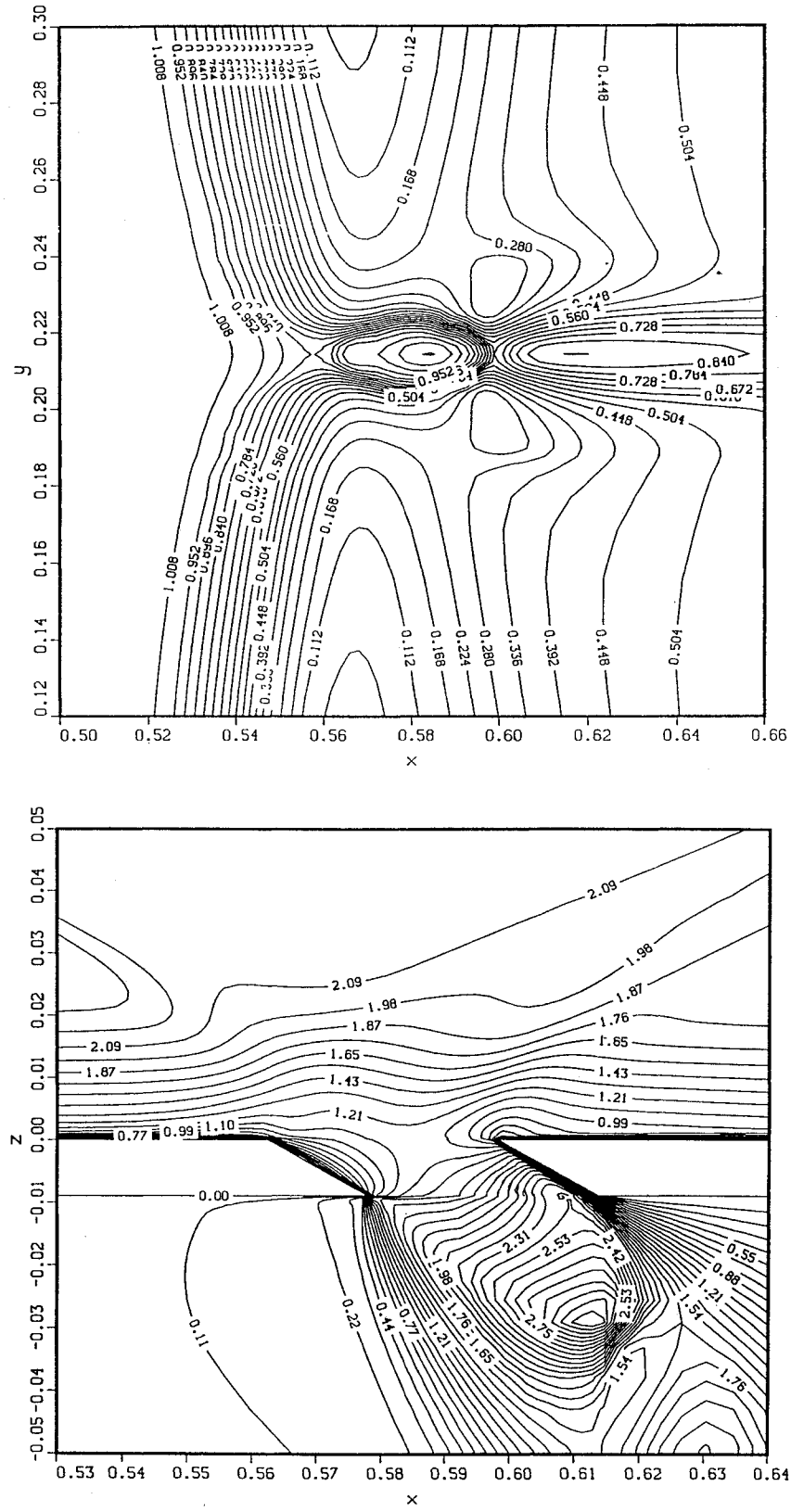


**Fig. 4 Mach number contours near the bleed hole for the case with a single 30-deg bleed hole and $P_b/P_\infty = 0.3$, top and side views.**

size that would form in the absence of bleed at a distance far from the bleed hole. These figures also show that a bleed hole can create a blast wave with the one produced by the 30-deg hole having larger spanwise gradients than the one produced by the 90-deg hole. The blast wave is created by the segment of the barrier shock above the flat plate. Air that passed through this segment of the barrier shock are at a pressure and Mach number different from those of the surrounding air that did not pass through it. Note that both the Mach number and pressure just downstream of the bleed hole are higher than those of the surrounding air. The reason for the higher pressure is expected since static pressure rises across a shock. The reason for the higher Mach number is less obvious. Although Mach number decreases across a shock, the Mach number can still be higher than those of the surrounding air because it was higher to begin with. The stream of air that passed through the top segment of the barrier shock had a Mach number that is higher than those of the

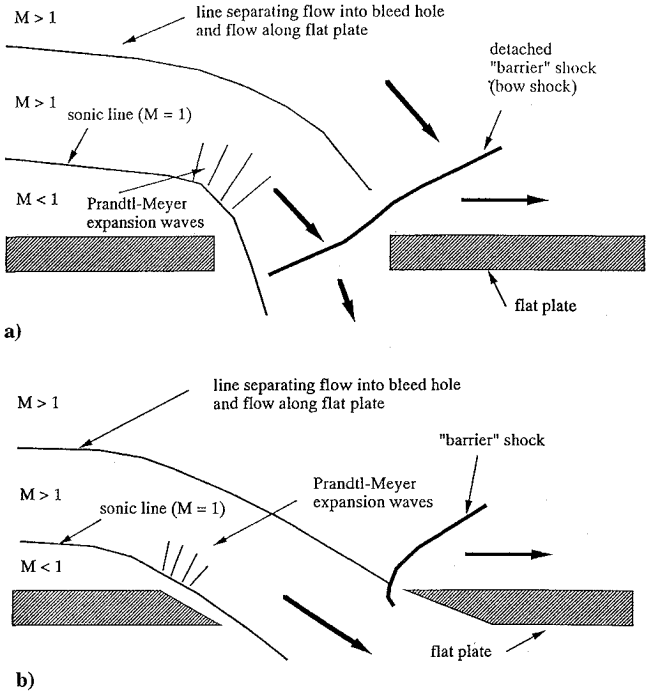


**Fig. 5 Schematic diagram of barrier shock: a) for 90-deg hole and b) for 30-deg hole.**

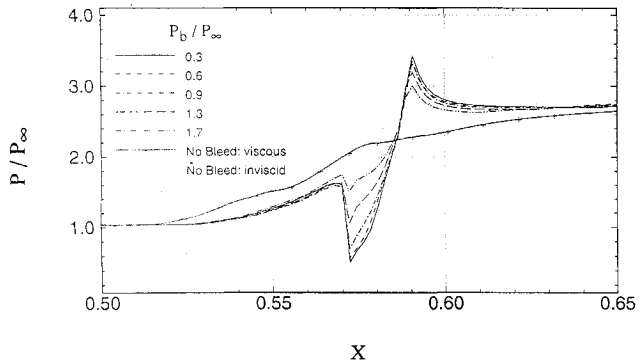


**Fig. 6 Pressure along wall from inflow to outflow passing through center of bleed hole for a single 90-deg bleed hole.**

surrounding air because it was initially farther away from the flat plate and was drawn to the plate by the bleed process.

Another important effect of the bleed-hole angle can be seen by examining the pressure distributions shown in Figs. 6 and 7. Note that the upstream influence length and adverse pressure gradient for the 30-deg hole are smaller than those for the 90-deg hole. This can be understood by noting that the 30-deg hole has a larger cross-sectional area parallel to the flat plate than the 90-deg hole even though both holes have the same "actual" cross-sectional area. This larger cross-sectional area at the plate surface enabled the 30-deg hole to start bleeding at a location farther upstream than that for the 90-deg hole.

Still another effect of bleed-hole angle is the difference in bleed flow coefficient and, hence, bleed rate. Figures 8 and 9 show the flow coefficient as a function of $P_b/P_s$, where $P_s$ is the average static pressure over the bleed hole when there is no bleed ($P_s$ has a different value over a different bleed hole due to the incident and the reflected shock waves).

Figures 8 and 9 show that with the same pressure ratio, a 30-deg hole has a flow coefficient that is almost twice that produced by a 90-deg hole. The lower flow coefficient and, hence, bleed rate in the 90-deg hole is caused by the presence of a larger separation region in the hole which reduces the available cross-sectional area for bleed. With the 30-deg hole, this separation region is much smaller so that there is more cross-sectional area in the hole available for bleed. The difference in the flow coefficient is one reason why the spanwise and

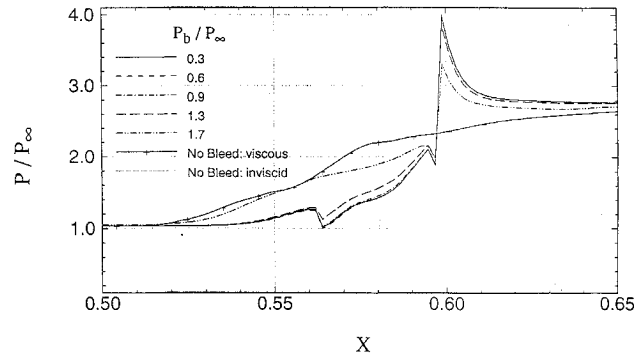


**Fig. 7 Pressure along wall from inflow to outflow passing through center of bleed hole for a single 30-deg bleed hole.**

downstream influence lengths for the 30-deg hole is greater than that for the 90-deg hole and why the strength of the barrier shock above the flat plate is also stronger for the 30-deg hole (see Figs. 3 and 4).

### Effects of an Upstream and a Downstream Bleed Hole

Figures 8–11 illustrate the effects of having an upstream and a downstream hole nearby. Figure 8 shows the effects of neighboring bleed holes on the flow coefficient or bleed rate for 90-deg holes. In Fig. 8, the single-hole data can only be compared with the second of 3 holes data because these two holes are located at the same location on the flat plate and, hence, are subjected to the same freestream pressure which is affected by the incident shock. Comparing data for these two holes shows that, except at very low-pressure ratios, the flow coefficient for an isolated hole is higher than that for the second hole, indicating that the flow coefficient is higher if there are no holes preceding it. The reason for this is as follows. When there is a preceding bleed hole, then that hole will remove most and possibly all of the subsonic part of the boundary layer. With a much thinner subsonic layer, the velocity vector of the supersonic flow above the flat plate will be almost parallel to the flat plate as it approaches the next bleed hole. This implies that this flow needs to turn a greater angle in order to enter into the bleed hole than is the case when the subsonic layer is thicker (note that a thicker subsonic layer will enable bending of supersonic flow to be started farther upstream of the bleed hole). A larger turning angle produces a larger separation region in the bleed hole which reduces the effective cross-sectional area available for bleed and, hence, lowers the flow coefficient. At very low-pressure ratios, the reverse can take place as far as the flow coefficient is concerned. This is because the barrier shock at the preceding bleed hole raises pressure and density which increase flow coefficient.

Figure 9 shows the effects of neighboring bleed holes on the flow coefficient or bleed rate for 30-deg holes. Similar to Fig. 8, the single-hole data can only be compared with the second of 3 holes data. Comparing data for these two holes shows that the flow coefficient for an isolated hole is lower than that for the second hole, indicating that the flow coefficient is higher if there are holes preceding it. This is the opposite of that for 90-deg holes. The reason for this is that, for 30-deg holes, the separation region formed in the bleed hole is always small so that the thickness of the subsonic layer plays a less important role in turning the supersonic flow into the bleed hole. In fact, for holes that do not have appreciable separated regions, the thickness of the boundary layer plays a different role on bleed rate. For such holes, the flow coefficient is higher when the boundary layer is thinner. This is because the flow inside the boundary layer must be bled before the flow outside of the boundary layer can be bled, and the flow inside the boundary layer has lower velocities than those outside of the boundary layer. Other parameters which affect the flow coefficient are the local density, static temperature, and static pressure. All of these parameters increase if there is a preceding hole with a barrier shock in it. Note that temperature is important in that it determines the sonic speed.

Figures 8 and 9 also show that when there are three holes, the flow coefficient through each hole can differ significantly from each other. In Fig. 9, it can be seen that, with 30-deg holes, the flow coefficient in the third hole is considerably higher than that in the second hole, which in turn is considerably higher than that in the first hole. In

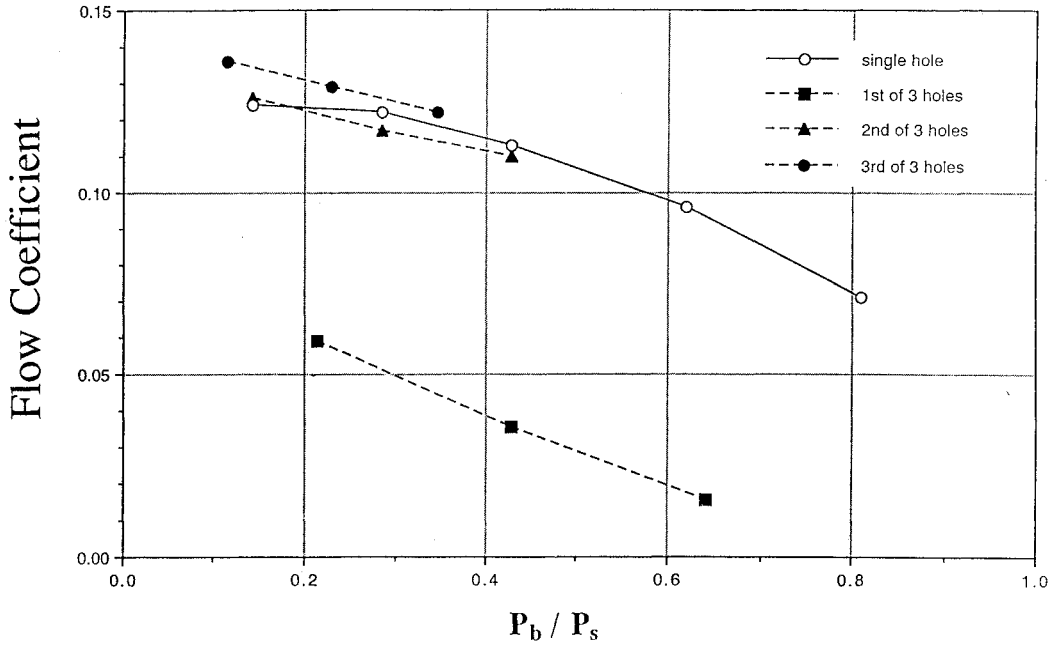


**Fig. 8 Flow coefficient as a function of $P_b/P_s$ for 90-deg bleed hole or holes.**

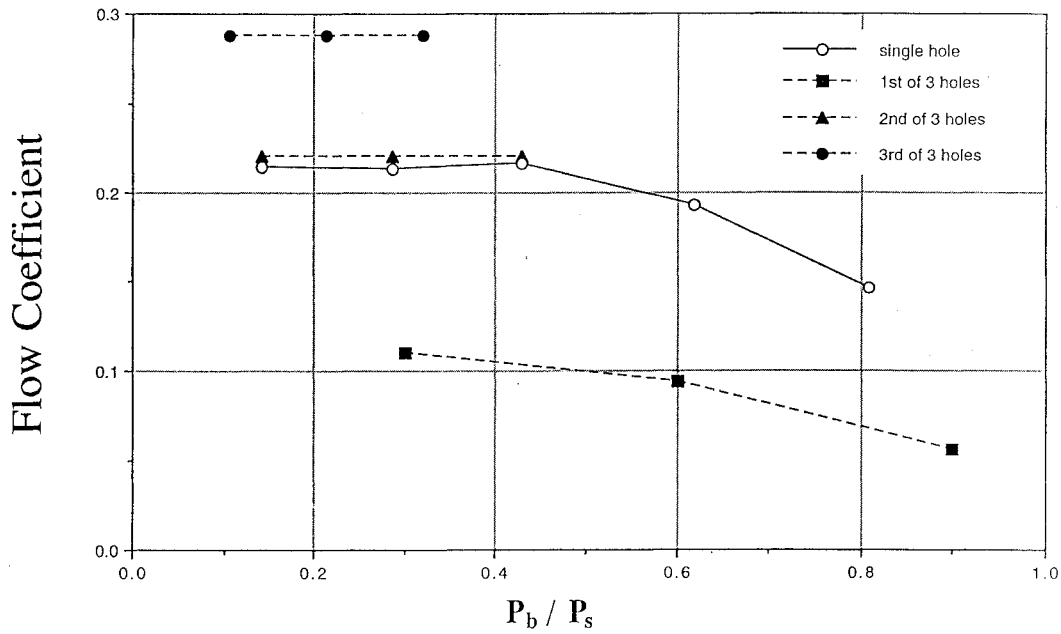


**Fig. 9 Flow coefficient as a function of $P_b/P_s$ for 30-deg bleed hole or holes.**

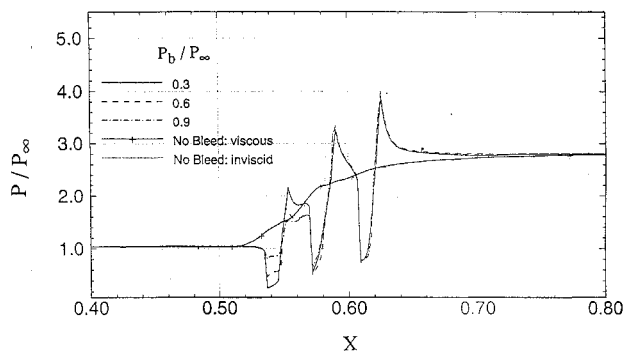


**Fig. 10 Pressure along wall from inflow to outflow passing through center of bleed hole for three 90-deg holes.**

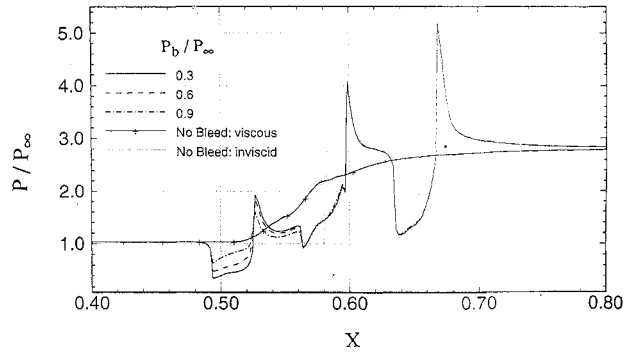


**Fig. 11 Pressure along wall from inflow to outflow passing through center of bleed hole for three 30-deg holes.**

Fig. 8, it can be seen that, with 90-deg holes, the difference in the flow coefficient through the second and third holes were considerably less than that for 30-deg holes. This is because the separation distance between 90-deg holes is less than that between 30-deg holes (i.e., $2D$ instead of $4D$). The increase in flow coefficient and hence bleed rate between the bleed holes can be attributed to two reasons. First, it is due to the rise in density, static pressure, and static temperature created by the incident shock wave and by the preceding barrier shock. Second, bleeding in preceding holes brought fluid with higher stagnation pressure and temperature closer to the wall surface to be bled by the next hole.

Figures 10 and 11 show the pressure distribution on the surface of the flat plate passing through the centers of the bleed holes. From these two figures, it can be seen that when there are three bleed holes, whether 30- or 90 deg, there are no upstream influence lengths. In fact, there are no adverse pressure gradients on the flat plate before the first bleed hole and after the second bleed hole. Between the first and second bleed holes, there is only a very mild adverse pressure gradient on the flat plate. All significant adverse pressure gradients were relegated to the region over the bleed holes where they cannot cause flow separations on the flat surface. The reason that the three-bleed-hole cases can completely eliminate adverse pressure gradient is that the first hole was placed upstream of where the incident shock wave impinged on the boundary layer so that the barrier shock in that bleed hole was able to prevent effects of the incident shock from propagating upstream.

Although results for the Mach number are not shown graphically when there are three bleed holes, two features are briefly noted. First, whether the bleed holes are 90 or 30 deg, each hole contains a barrier shock with a structure that depends on the bleed-hole angle. Second, the barrier shock in the middle hole is the weakest.

#### Effects of Pressure Ratio

The effects of the pressure ratio $P_b/P_\infty$ can be seen by examining Figs. 6–11. Figure 6 shows that for an isolated 90-deg hole, the pressure distribution on the surface of the flat plate is similar in trend for all pressure ratios investigated. Figure 7 shows that this is not the situation for an isolated 30-deg hole. With an isolated 30-deg hole, the surface pressure distribution does not exhibit a dip at the leading edge of the bleed hole when $P_b/P_\infty$ equalled 1.7. However, when $P_b/P_\infty$ is less than 0.9, the pressure distributions are identical.

Figure 8 shows that for 90-deg holes, the flow coefficient and, hence, bleed rate decreases as the pressure ratio $P_b/P_s$ increases. This result is expected for flows that are not choked. However, it should be noted that when there are three holes, only the flow coefficient through the first hole is significantly influenced by the pressure ratio. The flow coefficient through the second and third holes were less affected by the pressure ratio, indicating that they are nearly choked.

Figure 9 shows that for an isolated 30-deg hole, the flow coefficient is independent of the pressure ratio when $P_b/P_s$ is less than 0.43. This indicates that the flow in the bleed hole is under choked-like conditions for those pressure ratios (even though the sonic line may not be located in the bleed hole), and explains why the pressure distributions shown in Fig. 7 for those pressure ratios are identical. When there are three 30-deg holes, the flow through the second and third holes are also under choked-like conditions since the flow coefficients in those two holes are independent of pressure ratio. But, the flow is not choked in the first hole since the flow coefficient there changes with pressure ratio. The flow in the first hole is not choked because that hole is located upstream of where the incident shock wave impinged on the boundary layer so that the effective pressure drop across the first hole is less than that through the second and third holes.

Thus, Figs. 8 and 9 show that the critical pressure ratio required to achieve choked-like conditions through a hole depends on the bleed-hole angle. Bleed through 30-deg holes "choke" at a higher pressure ratio than those through 90-deg holes. One explanation for this behavior is as follows. The 90-deg holes contain large separation regions whereas the 30-deg holes do not. Also, for the 90-deg holes studied here with a diameter to thickness ratio of 2 (see Fig. 1), the separation region can extend from the bleed hole into the plenum. For 30-deg holes, the separation region being smaller is generally confined to within the bleed hole. If the separation region can extend beyond the bleed hole into the plenum, then increases in pressure ratio were found to decrease the size of the separation region even when the flow is supersonic outside of the separation region. This behavior is possible because the subsonic separation region allows pressure information in the plenum to be communicated to the separation region in the bleed hole through the part of the separation region that is contained in the plenum.

Figures 8 and 9 also show that except for the first bleed hole (i.e., the hole upstream of the impinging shock), the flow coefficient is about 7–14% for 90-deg holes and about 15–30% for 30-deg holes. Here, it is interesting to note that Chyu et al.[16] developed a bleed boundary condition for turbojet inlet computations which used a flow coefficient. In their study, the value of the flow coefficient used was 7% for a bleed surface with 40% porosity. This implies that for a 100% porous surface such as a hole, the flow coefficient would be 7%/40% or 17.5%, which is comparable to those obtained in this study for 90-deg holes at low-pressure ratios.

Figures 10 and 11 show the pressure distribution on the surface of the flat plate when there are three bleed holes. From these figures note that whether the holes are 30- or 90-deg, only the first hole was significantly affected by the pressure ratio. In fact for 30-deg holes, the pressure distribution over the second and third holes were independent of the pressure ratios investigated. The reason for this is that the flows through the second and third 30-deg hole were under choked-like conditions as explained earlier.

Finally, it is noted that the velocity vector plots not shown here indicate the following about flow separation. First, in the absence of bleed, the separation bubble had a length of $2.885D$ in the streamwise direction and a height of $0.139D$ in the direction normal to the flat plate. When there are three bleed holes, whether 90-deg or 30-deg ones, bleed was able to eliminate flow separation upstream and downstream of the hole for all pressure ratios studied. For an isolated 30-deg hole, bleed was also able to eliminate flow separation for all pressure ratios studied. But, this is not so with an isolated 90-deg hole. With an isolated 90-deg hole, flow separation remained when $P_b/P_\infty$ equalled 1.7. This result does not imply that an isolated 90-deg hole is less effective than an isolated 30-deg hole in controlling flow separation. What it does mean is that correct placement of an isolated 90-deg hole is more critical than that for an isolated 30-deg hole. This is because the cross-sectional area at the surface of the flat plate for a 30-deg hole is much larger than that for a 90-deg hole. Also, a 30-deg hole has a much higher bleed rate than a 90-deg hole. Note that the preceding discussion on the separation bubble and its elimination is confined to the region upstream and downstream of the bleed hole. As previously mentioned, the separation bubble persisted in the spanwise direction.

## Concluding Remarks

This three-dimensional numerical study showed how bleed-hole angle, presence of an upstream and a downstream bleed hole, and pressure ratio across bleed holes affect shock-wave/boundary-layer interactions on a flat plate. Based on this study, it was found that the structure of the barrier shock formed in the bleed holes by the bleed process is a strong function of the bleed-hole angle. Also, it was found that 90-deg holes can eliminate shock-wave induced flow separation with less bleed, but its placement is more critical. Since the bleed rate is more sensitive to pressure ratio for 90-deg holes, the usage of these holes permit more control. The 30-deg holes are not without merits. Even though 30-deg holes have higher bleed rates and allow less control, elimination of separation is more easily ensured. When there are multiple bleed holes with at least one bleed hole before the location where the incident shock wave strikes the boundary layer, there were no adverse pressure gradients on the flat plate.

## References

[1]Delery, J. M., "Shock Wave/Turbulent Boundary Layer Interaction and Its Control," *Progress in Aerospace Sciences*, Vol. 22, AIAA, New York, 1985, pp. 209–280.

[2]Hamed, A., and Shang, J., "Survey of Validation Data Base for Shock-wave Boundary Layer Interactions in Supersonic Inlets," *Journal of Propulsion and Power*, Vol. 7, No. 4, 1991, pp. 617–625.

[3]Hamed, A., and Lehnig, T., "An Investigation of Oblique Shock/Boundary Layer/Bleed Interaction," AIAA Paper 90-1928, July 1990.

[4]Hamed, A., and Lehnig, T., "The Effect of Bleed Configuration on Shock/Boundary Layer Interactions," AIAA Paper 91-2014, June 1991.

[5]Hamed, A., Shih, S. H., and Yeuan, J. J., "An Investigation of Shock/Turbulent Boundary Layer/Bleed Interactions," AIAA Paper 92-3085, July 1992.

[6]Hamed, A., Shih, S. H., and Yeuan, J. J., "A Parametric Study of Bleed in Shock Boundary Layer Interactions," AIAA Paper 93-0294, Jan. 1993.

[7]Hamed, A., Yeun, J. J., and Shih, S. H., "An Investigation of Shock Wave Turbulent Boundary Layer Interactions with Bleed through Slanted Slots," AIAA Paper 93-2992, July 1993.

[8]Hahn, T. O., Shih, T. I-P., and Chyu, W. J., "Numerical Study of Shock-Wave/Boundary-Layer Interactions with Bleed," *AIAA Journal*, Vol. 31, No. 5, 1993, pp. 869–876.

[9]Shih, T. I-P., Rimlinger, M. J., and Chyu, W. J., "Three-Dimensional Shock-Wave/Boundary-Layer Interaction with Bleed," *AIAA Journal*, Vol. 31, No. 10, 1993, pp. 1819–1826.

[10]Baldwin, B., and Lomax, H., "Thin Layer Approximation and Algebraic Model for Separated Turbulent Flows," AIAA Paper 78-257, Jan. 1978.

[11]Buning, P. G., and Chan, W. M., "OVERFLOW/F3D User's Manual," unpublished.

[12]Steger, J. L., and Warming, R. F., "Flux-Vector Splitting of the Inviscid Gasdynamic Equations with Application to Finite-Difference Methods," *Journal of Computational Physics*, Vol. 40, No. 2, 1981, pp. 263–293.

[13]Steger, J. L., Ying, S. X., and Schiff, L. B., "A Partially Flux-Split Algorithm for Numerical Simulation of Compressible Inviscid and Viscous Flow," *Proceedings of the Workshop on Computational Fluid Dynamics*, Inst. of Nonlinear Sciences, Univ. of Calif., Davis, CA, 1986.

[14]Vinokur, M., "On One-Dimensional Stretching Functions for Finite-Difference Calculations," *Journal of Computational Physics*, Vol. 50, No. 1, 1983, pp. 215–234.

[15]Benek, J. A., Buning, P. G., and Steger, J. L., "A 3-D Chimera Grid Embedding Technique," AIAA Paper 85-1523, July 1985.

[16]Chyu, W. J., Howe, G. W., and Shih, T. I-P., "Bleed Boundary Conditions for Numerically Simulated Mixed-Compression Supersonic Inlet Flow," *Journal of Propulsion and Power*, Vol. 8, No. 4, 1992, pp. 862–868 (AIAA Paper 88-0270).